Proceedings of the
Annual Stability Conference
Structural Stability Research Council
Atlanta, Georgia, April 21-24, 2026

Optimization of aluminum hollow sections using additive manufacturing

Juan-David Orozco[1], Carlos Graciano[2], Liya Li[3]

Abstract
Additive Manufacturing (AM), particularly Wire Arc Additive Manufacturing (WAAM), offers new opportunities for the fabrication of metal structural elements with complex geometries. This study focuses on the optimization of square hollow sections (SHS) and polygonal sections reinforced with stiffeners and internal walls, features that are difficult to achieve with conventional extrusion but can be easily realized through WAAM. By systematically analyzing existing studies on metal sections and WAAM-fabricated components, this work aims to identify how geometric modifications influence local buckling resistance, imperfection sensitivity, and overall stability. Numerical investigations are conducted to evaluate various stiffener configurations and internal wall layouts, highlighting their effectiveness in enhancing structural performance while minimizing additional material usage. The results provide design insights for creating lightweight, efficient, and robust aluminum profiles for demanding structural applications. Future experimental tests on WAAM-fabricated SHS and polygonal sections will validate these numerical findings and support the development of practical design recommendations for integrating AM technologies into structural engineering.

1. Introduction

Wire Arc Additive Manufacturing (WAAM) has recently emerged as a promising metal additive manufacturing technology for large-scale structural applications. Unlike powder-based additive manufacturing processes, WAAM utilizes an electric arc as the heat source and metal wire as feedstock, enabling high deposition rates, reduced material waste, and the fabrication of components at architectural and structural scales. These characteristics make WAAM particularly attractive for the construction industry, where geometric flexibility, customization, and efficient material usage are increasingly important design drivers (Gardner, 2023). The technology allows engineers to move beyond conventional manufacturing constraints and produce structurally efficient geometries that are difficult or impossible to achieve using traditional fabrication methods.

The feasibility of WAAM for civil engineering applications has been demonstrated through several pioneering projects and research initiatives. A notable example is the MX3D Bridge (see Fig. 1)

[1] PhD student, Université de Sherbrooke <juan.david.orozco@usherbrooke.ca>
[2] Full Professor, Universidad Nacional de Colombia <cagracianog@unal.edu.co >
[3] Assistant Professor, Université de Sherbrooke <liya.li@ usherbrooke.ca >

in Amsterdam, which represents one of the first full-scale load-bearing metallic structures produced using robotic WAAM technology (Kyvelou et al., 2022). Subsequent studies have explored WAAM applications in hybrid construction systems, optimized truss members, and complex structural connections (Laghi et al., 2024; Ye et al., 2021; Zuo et al., 2023). These investigations highlight the potential of WAAM to enable innovative structural forms while maintaining relatively low fabrication costs and reducing the need for extensive welding or assembly operations.

a) b) c)

Figure 1: Landmark application of WAAM in construction – a) Aluminum printed facade node (Strauss & Knaack, 2016) – b) Pedestrian bridge in Amsterdam (3D Metal Printing for Industrial Industry, n.d.) – c) Takenaka Connector in Japan (3D Metal Printing for Industrial Industry, n.d.)

Most existing WAAM research has focused on structural steels. Studies have demonstrated that WAAM enables the production of optimized members and architecturally integrated structural components by simultaneously considering material behaviour, manufacturing constraints, and structural performance. For example, Laghi et al. (2020) integrated architectural design concepts with manufacturing and mechanical considerations to develop a WAAM-fabricated diagrid column. Topology optimization approaches have also been applied to design truss members and cross-sections with improved capacity-to-mass ratios compared to conventional steel structures (Ye et al., 2021). Additional investigations on geometrically optimized shells, including wavy cylindrical shells and sinusoidally corrugated configurations, have shown significant improvements in load-carrying capacity and reduced sensitivity to geometric imperfections (Zhang et al., 2022). Within this context, WAAM enables the realization of advanced cross-sectional layouts incorporating tailored stiffening strategies that are difficult to achieve using traditional fabrication methods. Experimental and numerical studies on optimized square hollow sections and stiffened stub columns have shown that internal stiffeners can substantially enhance compressive resistance while introducing only moderate increases in structural mass (Meng et al., 2023). Collectively, these findings confirm that additive manufacturing supports a performance-driven structural design approach, enabling cross-sectional efficiencies that extend beyond the limitations of conventional rolled or welded steel profiles.

More recently, stainless steel WAAM has also attracted attention due to its corrosion resistance and suitability for architectural and infrastructure applications. Investigations on WAAM stainless steel components have explored the interaction between process parameters, microstructural evolution, and mechanical performance, confirming the feasibility of producing load-bearing structural elements while maintaining acceptable strength and ductility levels. These studies collectively demonstrate that WAAM is transitioning from a prototyping technology toward a viable manufacturing approach for structural engineering applications. Kyvelou et al. (2021)

conducted an extensive experimental study on 14 SHS WAAM stainless steel stub columns, with particular focus on the influence of initial geometric imperfections inherent to the manufacturing process. The results were benchmarked against current design standards (AISC 370 (American Institute of Steel Construction, 2021) and EC3 1993-1-4 (European Committee for Standardization, 2025)), revealing an unconservative prediction of the cross-section capacity. Huang et al. (2026) developed experimental and numerical studies on the comprehension of the local buckling development under compression loads for of open cross-sections (T-Shaped, channel and angle. Observed a strong correlation between the thermal gradients and geometric variabilities on the specimens. Also found that design codes (EC3 1993-1-4 and AISC 370) underestimate the compression resistance specially on the slender range for the WAAM sections.

Despite these advances in stee or stainless-steel based materials, the application of WAAM to aluminum structural systems remains comparatively underexplored. Aluminum alloys offer unique advantages such as high strength-to-weight ratios, excellent corrosion resistance resulting from the formation of a natural oxide layer, and exceptional formability. However, WAAM fabrication of aluminum presents additional challenges, including porosity formation, thermal sensitivity, microstructural instability, and variability in mechanical properties, which require further investigation (Sarıkaya et al., 2024). Existing studies have primarily focused on material characterization, particularly for alloys such as 2319 and 5356, examining deposition strategies and mechanical performance (Ye et al., 2025). Recent work by (Li et al., 2026) investigated the post-fire mechanical behaviour of WAAM-fabricated 5356 aluminum alloy plates with different deposition orientations, demonstrating the feasibility of the process for structural applications. Nevertheless, systematic research linking aluminum WAAM manufacturing, cross-section optimization, and structural stability performance is still lacking, highlighting a critical research gap that must be addressed before widespread structural implementation can be achieved.

In this paper, the research explores the potential of aluminum structural cross-sections fabricated using WAAM, with particular emphasis on Square Hollow Sections (SHS), and polygonal sections incorporating internal stiffeners subjected to compression. The study aims to evaluate the feasibility of exploiting WAAM manufacturing capabilities to develop structurally efficient aluminum sections with enhanced stability performance. Section 2 presents the development of detailed finite element (FE) numerical models capable of capturing the material and geometric characteristics of WAAM-fabricated sections. Section 3 and 4 describes an extensive parametric study investigating the influence of key geometric parameters, stiffening configurations, and slenderness on the structural response and buckling resistance. Complementary experimental tests are currently being prepared and will be conducted in the near future to validate the numerical findings and further assess the structural behavior of aluminum WAAM members under compression.

2. Numerical Models

Hollow sections with internal stiffeners subjected to compressive loading were analysed using the nonlinear FE software ABAQUS (ABAQUS, 2011). The numerical models were developed following modelling strategies previously validated for aluminum structural members and WAAM-fabricated components. Shell element S4R, a four-node doubly curved reduced-integration element with finite membrane strains, was adopted due to its proven accuracy and

computational efficiency in capturing local buckling and post-buckling behavior of thin-walled aluminum sections (Dahboul et al., 2023; Zhao et al., 2019).

The modelling procedure consisted of two sequential analyses. First, Linear Buckling Analyses (LBA) were performed to obtain the elastic critical buckling loads and associated eigenmodes. The first buckling eigenmode was subsequently introduced as the initial geometric imperfection for the nonlinear analyses. Second, Geometric and Materially Nonlinear Analyses with Imperfections (GMNIA) were carried out to evaluate the ultimate compressive resistance and post-buckling response of the sections. In the present study, the imperfection amplitude was assumed as $\frac{t}{2000}\left(\frac{D}{t}\right)^{1.5}$, consistent with values commonly adopted in previous numerical investigations of aluminum thin-walled sections (Echeverri et al., 2024) where the D is the external perimeter, t is thickness. This assumption provides a reasonable representation of fabrication-induced imperfections; however, the adopted imperfection amplitude will be refined and calibrated in future work based on forthcoming experimental measurements.

A mesh sensitivity study was conducted to ensure numerical accuracy. The adopted mesh size corresponds approximately to $D/100$ (see Fig. 2) while guaranteeing a minimum of six shell elements per plate segment along each side of the section. This discretization was found sufficient to accurately capture local buckling development without excessive computational cost.

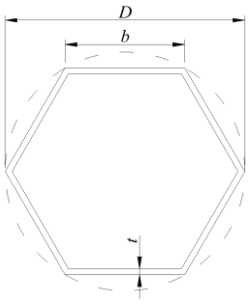

Figure 2: Calibration parameters for SHS and polygonal sections

The material response of the aluminum alloys was derived from the Ramberg–Osgood formulation, allowing proper representation of the gradual yielding and strain-hardening characteristics typical of aluminum alloys. The adopted material curves, described in Table 1, were calibrated to reproduce nonlinear material behaviour suitable for stability analyses. In this study, four aluminum alloys were considered, including alloy 5356, which is commonly used in WAAM fabrication, together with three conventional 6000-series alloys widely employed in civil engineering applications. The selected materials allow comparison between WAAM-compatible aluminum and traditionally extruded structural alloys, enabling assessment of the influence of material properties on the structural performance and stability behavior of the investigated cross-sections. Note that, compared with the 6000-series alloys, alloy 5356 exhibits a lower yield strength f_y; however, it benefits from a more pronounced strain-hardening response and higher ductility, characterized by greater elongation capacity.

Table 1: Mechanical properties aluminum alloys

Alloy[1]	$f_{0.2}$ [MPa]	f_u [MPa]	E [MPa]	n [-]	Elongation [%]
6063-T6	170	220	70000	19.5	0.08
6082-T6	260	320	70000	20.7	0.08
6061-T6	240	260	70000	55.0	0.08
5356	119	255	70000	6.0	0.15

The boundary conditions adopted in the numerical models represent simply supported conditions as presented in Fig. 3. One end of the member was restrained against all translational degrees of freedom and rotation about the longitudinal axis $(u_x = u_y = u_z = \theta_x = 0)$, while the opposite end allowed axial displacement but prevented transverse displacements and torsional rotation $(u_y = u_z = \theta_x = 0)$. The compressive load was applied through a reference point located at the centroid of the cross-section. The reference point was coupled to the end section using a rigid body constraint, ensuring uniform load transfer and preventing local stress concentrations at the loading interface.

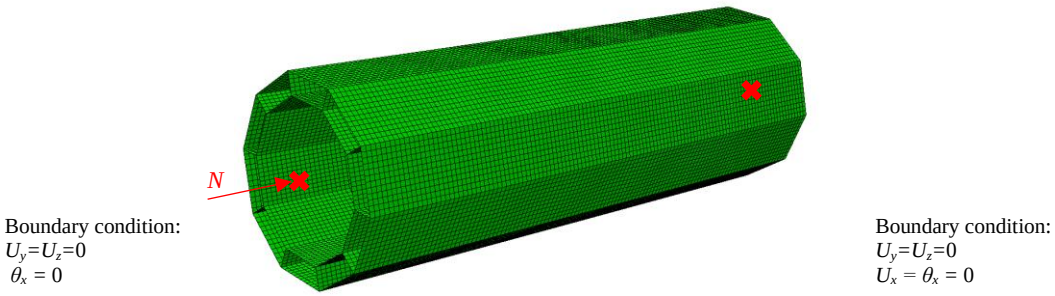

Figure 3: Boundary conditions in numerical models

3. Parametric studies

A comprehensive parametric study was conducted to investigate the compressive behaviour of advanced aluminum hollow sections. In total, six types of cross-sectional geometries were examined. These included five families of Double-Wall Stiffened Polygonal (DWP) sections with different numbers of sides, namely 4-, 6-, 8-, 10-, and 12-sided configurations (see Fig. 4). In addition, for the octagonal configuration, a recently developed structural form (Chehrazad et al., 2023), the Internal-Stiffened Octagonal (ISO) section, was also investigated. The ISO section has been recently proposed for aluminum transmission tower applications to enhance stability and structural efficiency. For each section type, multiple stiffener arrangements were considered in order to evaluate the influence of stiffener layout on buckling behaviour and ultimate resistance. The geometrical configurations and stiffener layouts are summarized in Fig. 5 and Table 2 and Table 3, where l_{stif} denotes the stiffener length for the DWP sections, b_{corner} represents the projected distance to the octagonal side, and b_{stif} corresponds to the distance from the corner to the internal stiffener.

In addition, a wide range of cross-section slenderness values was examined for each configuration by varying wall thicknesses and geometric proportions, allowing both stocky and slender members to be represented. Overall, a total of 5040 numerical models were developed and analysed using GMNIA to evaluate ultimate compressive resistance and post-buckling response.

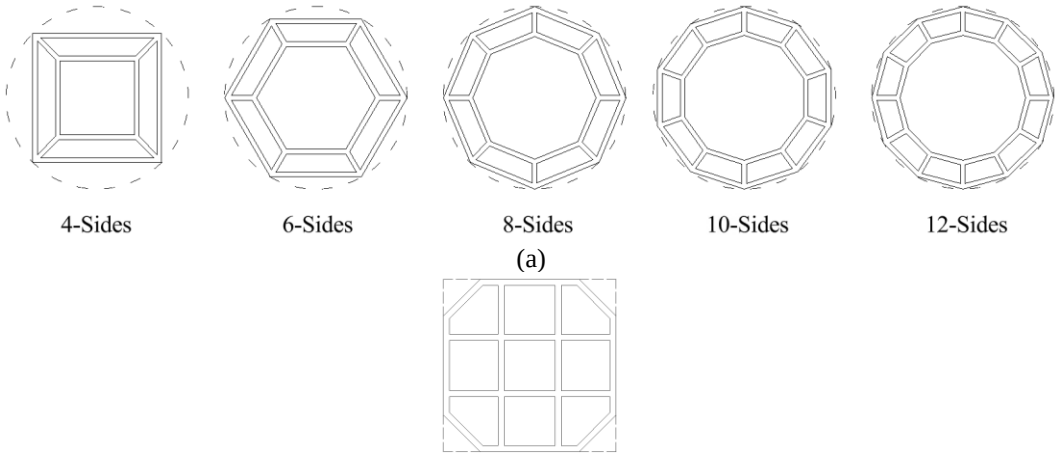

Figure 4: Types of internal stiffened sections studied – a) DWP -b) ISO

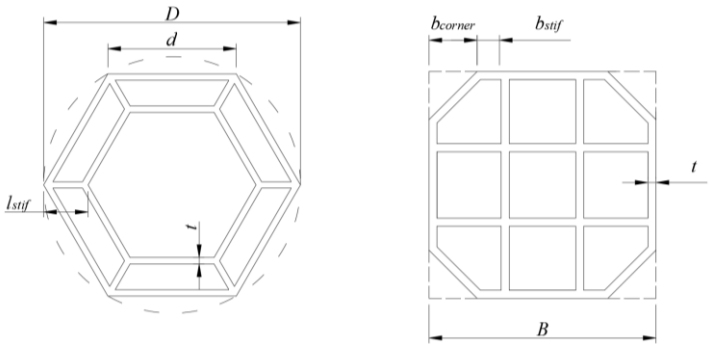

Figure 5: Geometry and notation for polygon stiffened sections – a. DWP section – b. ISO section

Table 2: Parametric study DWP sections

Parameter	Range	
D	25.0 – 160.0	mm
t	1.2 – 8.0	mm
d	6.50 - 113.15	mm
D/t	12.0 – 106.7	-
l_{stif} / D	0.10; 0.15; 0.20	-

Table 3: Parametric study ISO sections

Parameter	Range	
B	17.5 - 113.0	mm
t	1.2 - 8.0	mm
B/t	9.8 - 75.4	-
b_{corner} / B	0.15 - 0.20	-
b_{stif} / B	0.10; 0.15; 0.20	-

4. Numerical Results

The results of the parametric study are presented in this section using a slenderness-based cross-section resistance format. The horizontal axis represents the cross-section slenderness, λ_L, as defined as $\lambda_L = \sqrt{f_{0.2} A / N_{cr}}$, where N_{cr} is the elastic critical load obtained from LBA performed

in ABAQUS, $f_{0.2}$ (taken as the 0.2% proof stress) is the material yield strength, and A is the cross-sectional area. The vertical axis corresponds to the normalized ultimate resistance, expressed as $N_{u,\mathrm{FE}}/(f_{0.2}A)$, where $N_{u,\mathrm{FE}}$ denotes the ultimate resistance obtained from the GMNIA.

Fig. 6 presents the comparison of the numerical results obtained for different aluminum alloys for the 10-sided DWP sections with $L_{\mathrm{stif}}/D = 0.10$and the ISO sections with $B_{\mathrm{corner}}/B = 0.15$ and $B_{\mathrm{stiff}}/B = 0.10$, as illustrated in Fig. 7 (a–b). A clear difference in structural response is observed between alloy 5356 and the conventional 6000-series alloys. Alloy 5356 exhibits a distinct trend due to its pronounced strain-hardening capacity and higher strength ratio $f_u/f_{0.2}$ compared with the 6000-series alloys. As a result, both DWP and ISO sections fabricated with alloy 5356 develop significant post-yield resistance, with normalized resistances exceeding 1.0 and reaching values up to approximately 2.7, while occurring at relatively low cross-section slenderness values, indicating generally more compact sections.

In contrast, the 6000-series alloys (6061-T6, 6063-T6, and 6082-T6) also benefit from strain hardening, although to a lesser extent. Their normalized resistances generally remain above unity and reach maximum values around 1.6, while stable resistance is maintained up to larger cross-section slenderness values approaching $\bar{\lambda}_L \approx 0.9$. It should be emphasized that current aluminum design standards neglect strain-hardening effects in compression member design, which leads to systematically conservative resistance predictions. This conservatism becomes particularly significant for WAAM-fabricated alloy 5356 sections, where strain hardening provides substantial additional load-carrying capacity beyond the nominal yield-based resistance.

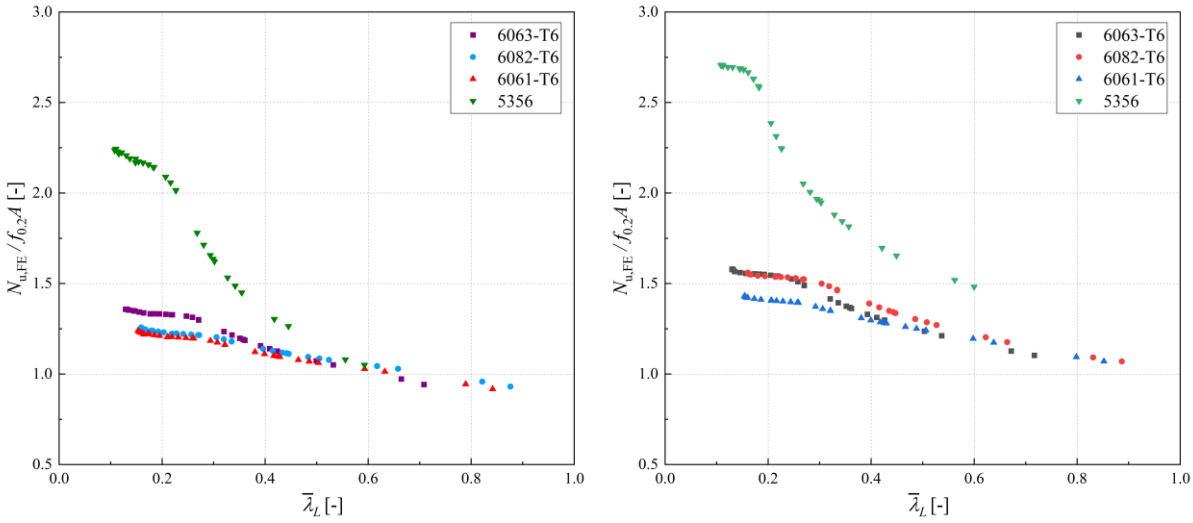

Figure 6: Influence of the aluminum alloy type on the normalized compressive resistance
(a) DWP with L_{stif}/D=0.10 (b) ISO B_{corner}/B=0.15 B_{stiff}/B=0.10

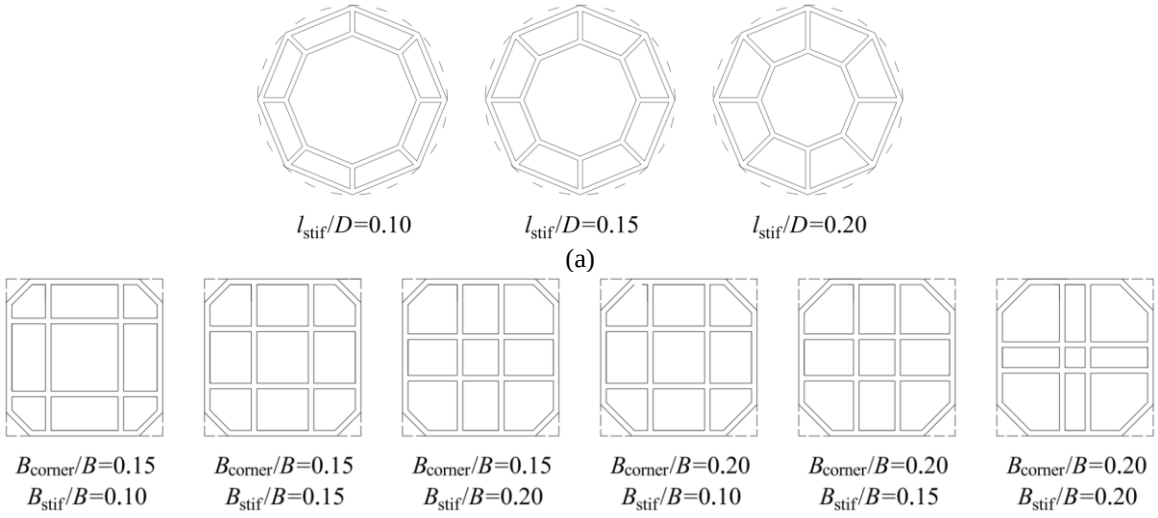

Figure 7: Influence of aluminum (a) DWP Sections (b) ISO Sections

Fig. 8 presents the influence of the number of sides of DWP sections with $L_{\text{stif}}/D = 0.10$ sections for alloys 6061-T6 (Fig. 8-a) and 5356 (Fig. 8-b). The investigated geometries range from four-sided sections (SHS) to 12-sided sections (dodecagonal sections), which progressively approach the behaviour of square hollow sections.

With the increase in the number of wall sides, the cross-sections become increasingly compact. A clear reduction in cross-section slenderness $\bar{\lambda}_L$ is observed, decreasing from approximately 2.0 to 0.8 for alloy 6061-T6 and from about 1.4 to 0.5 for alloy 5356. This evolution reflects a gradual transition from plate-dominated buckling behaviour in SHS sections toward shell-like buckling behaviour in multi-sided polygonal sections. Correspondingly, the normalized cross-section resistance increases as the number of sides increases, indicating improved stability performance for geometries approaching circular configurations.

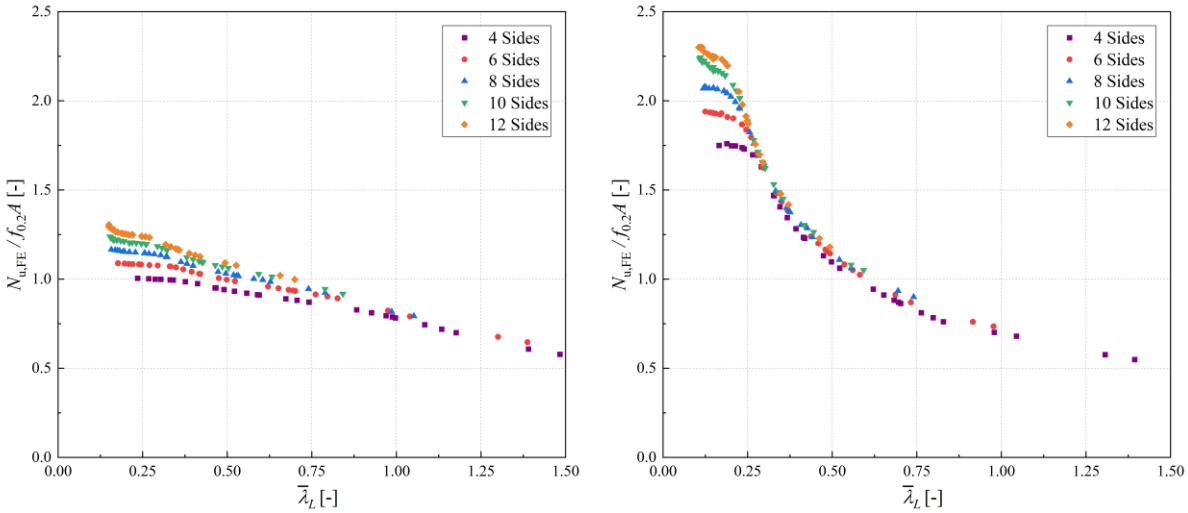

Figure 8: Influence of the number of sides for DWP sections on compressive resistance
(a) Alloy 6061-T6 (b) Alloy 5356

Fig. 9 further compares DWP sections with 4 sides (SHS) and 12 sides (dodecagon) incorporating three stiffener configurations with $L_{stif}/D = 0.10$, 0.15, and 0.20. For SHS sections, the influence of stiffener spacing remains limited and becomes noticeable mainly for slender sections with $\bar{\lambda}_L > 0.7$. In these cases, larger L_{stif}/Dratios lead to slightly higher normalized resistances, likely due to improved restraint against local plate buckling.

In contrast, for alloy 5356, which exhibits pronounced strain-hardening behaviour, a stronger influence of the stiffener configuration is observed for dodecagonal sections, particularly at low slenderness levels ($\bar{\lambda}_L \approx 0.2$). The enhanced resistance in these compact sections is attributed to the combined effects of delayed local instability and significant post-yield strain hardening, which become increasingly dominant as the geometry approaches shell behaviour.

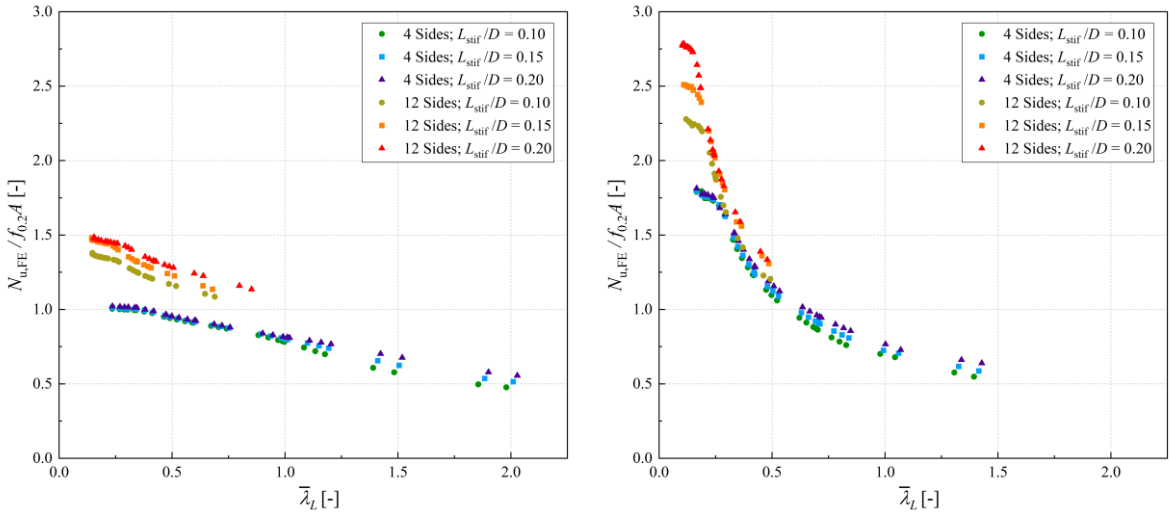

Figure 9: Comparison of normalized compression resistance between DWP sections 4 and Sides and 12 (a) Alloy 6061-T6 (b) Alloy 5356

Fig. 10 presents the influence of different stiffener configurations for the ISO sections. Six configurations were considered, combining $B_{\text{corner}}/B = 0.15$ and 0.20 with $B_{\text{stiff}}/B = 0.10$, 0.15, and 0.20. As the ratio B_{corner}/B increases, the ISO geometry progressively approaches that of a standard octagonal section. Simultaneously, increasing both B_{corner}/B and B_{stiff}/B shifts the internal walls closer toward the section center, as illustrated in Fig. 7.

The results indicate that higher normalized resistances are generally achieved for lower combinations of B_{corner}/B and B_{stiff}/B. The difference in nominal resistance between the configuration with $B_{\text{corner}}/B = 0.15$ and $B_{\text{stiff}}/B = 0.10$ and that with $B_{\text{corner}}/B = 0.20$ and $B_{\text{stiff}}/B = 0.20$ can reach approximately 40%. This demonstrates that the stiffener arrangement has a significant influence on structural efficiency and should be explicitly considered when optimizing cross-sectional geometries.

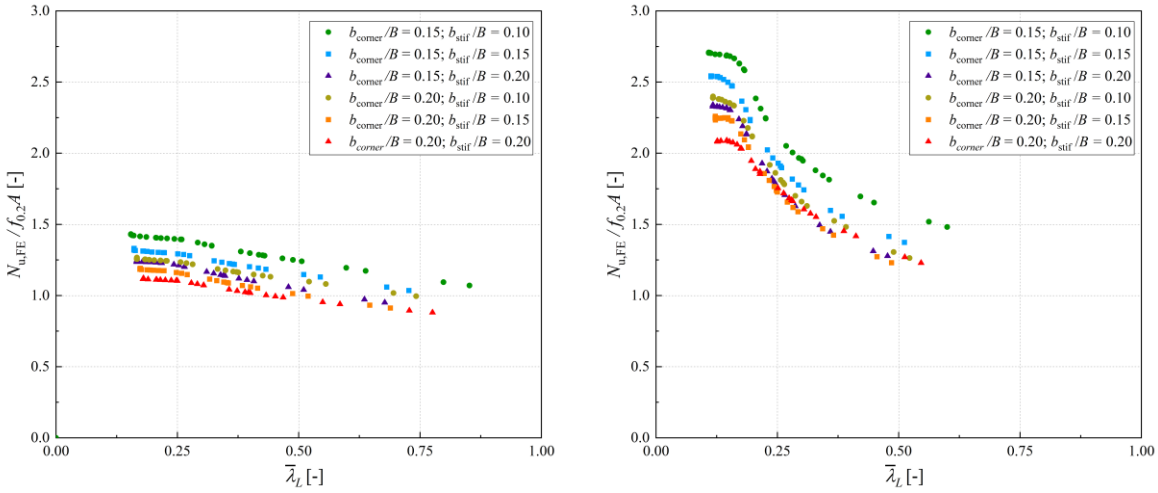

(a) (b)

Figure 10: Comparison of normalized compression resistance for ISO sections with different b_{corner}/B and b_{stif}/B ratios
(a) Alloy 6061-T6 (b) Alloy 5356

Fig. 11 further compares the influence of stiffener configurations for ISO and DWP eight-sided (octagonal) sections. The results show that, for both section types, variations in stiffener arrangement significantly affect the normalized cross-section resistance. However, a wider range of resistance scatter is observed for the ISO sections due to changes in the B_{corner}/B and B_{stiff}/B ratios, indicating a stronger sensitivity of ISO geometries to stiffener layout.

In contrast, the DWP sections generally exhibit slightly lower normalized resistance and comparatively higher cross-section slenderness values, particularly in the slender range, when compared with ISO sections having $B_{\text{corner}}/B = 0.15$. These observations suggest that, under certain geometric configurations, ISO sections may achieve higher structural efficiency than DWP sections, highlighting the importance of cross-sectional topology in optimizing stability performance.

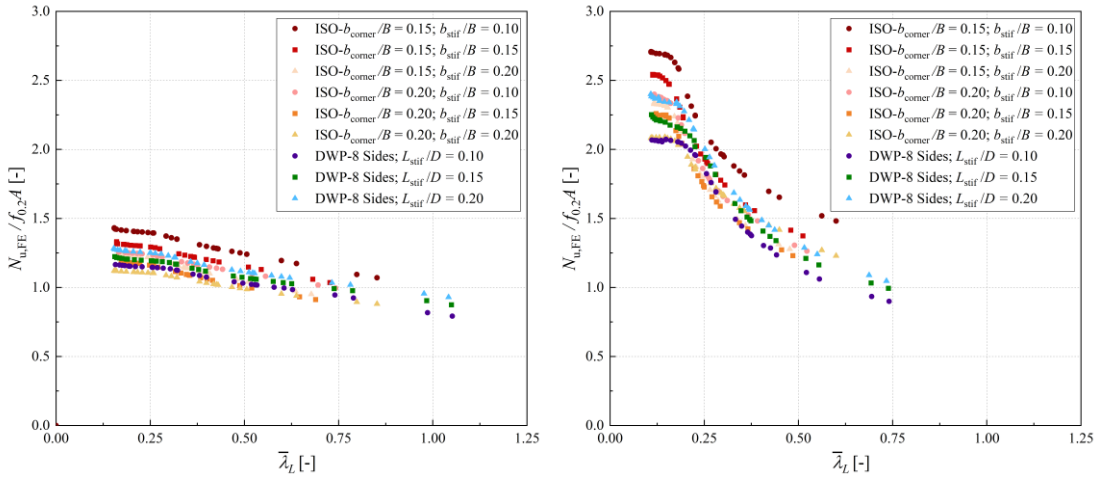

(a) (b)

Figure 11: Comparison of normalized compression resistance between DWP 8 sides and ISO sections
(a) Alloy 6061-T6 (b) Alloy 5356

4. Conclusions

This study investigated the stability behaviour and compressive resistance of optimized aluminum polygonal sections through extensive numerical parametric analyses. The influence of alloy type, number of cross-section sides, and stiffener configurations was systematically examined using nonlinear FE modelling.

The results demonstrate that material properties play a decisive role in structural performance. Alloy 5356 exhibits a markedly different response compared with conventional 6000-series alloys due to its pronounced strain-hardening capacity and higher $f_u/f_{0.2}$ ratio. Significant post-yield strength development was observed, with normalized resistances exceeding unity and reaching values well above those predicted by current design standards. These findings indicate that existing aluminum design provisions, which neglect strain hardening effects, will lead to conservative resistance predictions, particularly for WAAM-fabricated structural members.

Geometric parameters were also shown to strongly influence stability behaviour. Increasing the number of cross-section sides results in more compact sections and a clear transition from plate-type buckling to shell-like buckling behaviour, accompanied by increased resistance. Furthermore, stiffener configuration significantly affects structural efficiency. For both DWP and ISO geometries, optimized combinations of corner and stiffener dimensions can produce substantial resistance gains, highlighting the importance of integrated geometric optimization rather than considering individual parameters independently.

Future Work

To validate the numerical findings, an experimental campaign is currently underway. Aluminum alloy 5356 specimens fabricated using WAAM technology have been produced, including square hollow sections (4 sides), hexagonal sections (6 sides), octagonal sections (8 sides), and circular hollow sections as shown in Fig. 12. Both unstiffened and stiffened configurations have been manufactured to investigate the combined influence of geometry and stiffener layout on structural performance.

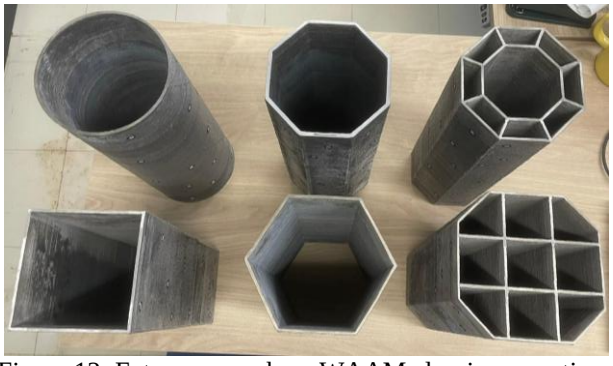

Figure 12: Future research on WAAM aluminum sections

Prior to testing, high-resolution 3D scanning (see Fig. 13) has been conducted to characterize geometric imperfection patterns and amplitudes. The measured imperfections will be used to establish realistic imperfection models for numerical simulations and to quantify the influence of manufacturing-induced imperfections on buckling behaviour. Upcoming experimental tests will focus on compressive resistance and post-buckling response, enabling direct validation of the

proposed numerical models and supporting the development of improved design recommendations for optimized aluminum structural sections.

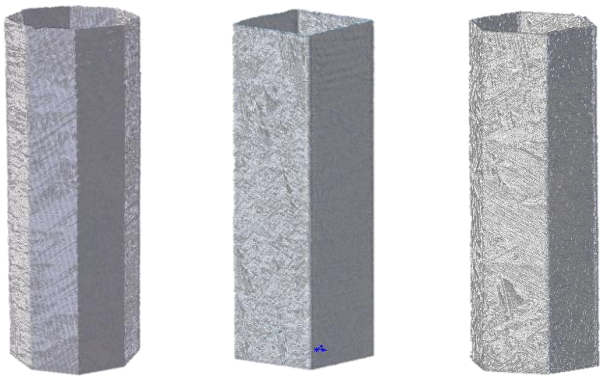

Figure 13: 3D Scanned polygonal WAAM aluminum specimens

References

3D metal printing for industrial Industry. (n.d.). MX3D. Retrieved July 6, 2025, from https://mx3d.com/industries/

ABAQUS. (2011). *Abaqus* (Version Abaqus 6.11). Dassault Systemes Simulia Corporation.

American Institute of Steel Construction. (2021). *Specification For Structural Stainless Steel Buildings*.

Chehrazad, S., Mohebbi, S., Lamarche, C.-P., Langlois, S., Desrochers, A., & Talatahari, S. (2023). Design and Optimization of Aluminum Member's Sections for Building Efficient 120–160 kV Power Transmission Towers. *Engineering Proceedings*, *43*(1), 5. https://doi.org/10.3390/engproc2023043005

Dahboul, S., Li, L., Coderre, T., & Boissonnade, N. (2023). O.I.C.-based design of extruded and welded aluminum I-sections. *Structures*, *58*, 105504. https://doi.org/10.1016/j.istruc.2023.105504

Echeverri, M., Rico, P., Li, L., Graciano, C., & Boissonnade, N. (2024, March 19). On the definition of geometrical imperfections in the F.E. modelling of CHS in compression. *Proceedings of the Annual Stability Conference*. Annual Stability Conference, San Antonio, Texas. https://www.ssrcweb.org/2024stabilityconferenceproceedings

European Committee for Standardization. (2025). *Eurocode 3 – Design of Steel Structures – Part 1.4: General rules – Supplementary rules For Stainless Steels*.

Gardner, L. (2023). Metal additive manufacturing in structural engineering – review, advances, opportunities and outlook. *Structures*, *47*, 2178–2193. https://doi.org/10.1016/j.istruc.2022.12.039

Huang, X., Wang, Z., Zhong, Y., Chen, M.-T., & Zhao, O. (2026). Cross-section compressive performance of wire arc additively manufactured stainless steel singly symmetric (T-shaped, channel and angle) section stub columns. *Thin-Walled Structures*, *223*, 114618. https://doi.org/10.1016/j.tws.2026.114618

Kyvelou, P., Buchanan, C., & Gardner, L. (2022). Numerical simulation and evaluation of the world's first metal additively manufactured bridge. *Structures*, *42*, 405–416. https://doi.org/10.1016/j.istruc.2022.06.012

Kyvelou, P., Huang, C., Gardner, L., & Buchanan, C. (2021). Structural Testing and Design of Wire Arc Additively Manufactured Square Hollow Sections. *Journal of Structural Engineering*, *147*(12), 04021218. https://doi.org/10.1061/(ASCE)ST.1943-541X.0003188

Laghi, V., Babovic, N., Benvenuti, E., & Kloft, H. (2024). Blended structural optimization of steel joints for Wire-and-Arc Additive Manufacturing. *Engineering Structures*, *300*, 117141. https://doi.org/10.1016/j.engstruct.2023.117141

Laghi, V., Palermo, M., Gasparini, G., & Trombetti, T. (2020). Computational design and manufacturing of a half-scaled 3D-printed stainless steel diagrid column. *Additive Manufacturing*, *36*, 101505. https://doi.org/10.1016/j.addma.2020.101505

Li, J., Jiang, K., Chen, M.-T., Wang, Z., Zhao, O., & Gardner, L. (2026). Mechanical properties and constitutive modelling of wire arc additively manufactured aluminium alloy after exposure to elevated temperatures. *Thin-Walled Structures*, *218*, 114119. https://doi.org/10.1016/j.tws.2025.114119

Meng, X., Weber, B., Nitawaki, M., & Gardner, L. (2023). Optimisation and testing of wire arc additively manufactured steel stub columns. *Thin-Walled Structures*, *189*, 110857. https://doi.org/10.1016/j.tws.2023.110857

Sarıkaya, M., Başcıl Önler, D., Dağlı, S., Hartomacıoğlu, S., Günay, M., & Królczyk, G. M. (2024). A review on aluminum alloys produced by wire arc additive manufacturing (WAAM): Applications, benefits, challenges and

future trends. *Journal of Materials Research and Technology*, *33*, 5643–5670. https://doi.org/10.1016/j.jmrt.2024.10.212

Strauss, H., & Knaack, U. (2016). Additive Manufacturing for Future Facades. *Journal of Facade Design and Engineering*, *3*. https://doi.org/10.7480/jfde.2015.3-4.875

Ye, J., Kyvelou, P., Gilardi, F., Lu, H., Gilbert, M., & Gardner, L. (2021). An End-to-End Framework for the Additive Manufacture of Optimized Tubular Structures. *IEEE Access*, *9*, 165476–165489. https://doi.org/10.1109/ACCESS.2021.3132797

Ye, J., Yang, R., Liu, Y., Quan, G., Wang, Z., & Zhao, Y. (2025). Stress-strain characterization of wire and arc additively manufactured aluminium alloys using the Ramberg-Osgood model. *Journal of Building Engineering*, *105*, 112519. https://doi.org/10.1016/j.jobe.2025.112519

Zhang, R., Meng, X., & Gardner, L. (2022). Shape optimisation of stainless steel corrugated cylindrical shells for additive manufacturing. *Engineering Structures*, *270*, 114857. https://doi.org/10.1016/j.engstruct.2022.114857

Zhao, Y., Zhai, X., & Wang, J. (2019). Buckling behaviors and ultimate strengths of 6082-T6 aluminum alloy columns under eccentric compression – Part I: Experiments and finite element modeling. *Thin-Walled Structures*, *143*, 106207. https://doi.org/10.1016/j.tws.2019.106207

Zuo, W., Chen, M.-T., Chen, Y., Zhao, O., Cheng, B., & Zhao, J. (2023). Additive manufacturing oriented parametric topology optimization design and numerical analysis of steel joints in gridshell structures. *Thin-Walled Structures*, *188*, 110817. https://doi.org/10.1016/j.tws.2023.110817